ACSNANO

www.acsnano.org

ARTICLE

Direct Current Fabric Triboelectric Nanogenerator for Biomotion Energy Harvesting

Chaoyu Chen,[#] Hengyu Guo,[#] Lijun Chen,[#] Yi-Cheng Wang, Xianjie Pu, Weidong Yu, Fumei Wang, Zhaoqun Du,[*] and Zhong Lin Wang[*]

Cite This: https://dx.doi.org/10.1021/acsnano.0c00138

Read Online

ACCESS | Metrics & More | Article Recommendations | Supporting Information

ABSTRACT: Triboelectric nanogenerators (TENGs) have demonstrated their promising potential in biomotion energy harvesting. A combination of the TENG and textile materials presents an effective approach toward smart fabric. However, most traditional fabric TENGs with an alternating current (AC) have to use a stiff, uncomfortable, and unfriendly rectifier bridge to obtain direct current (DC) to store and supply power for electronic devices. Here, a DC fabric TENG (DC F-TENG) with the most common plain structure is designed to harvest biomotion energy by tactfully taking advantage of the harmful and annoying electrostatic breakdown phenomenon of clothes. A small DC F-TENG (1.5 cm × 3.5 cm) can easily light up 416 serially connected light-emitting diodes. Furthermore, some yarn supercapacitors are fabricated and woven into the DC F-TENG to harvest and store energy and to power electronic devices, such as a hygrothermograph or a calculator, which shows great convenience and high efficiency in practice. This low-cost and efficient DC F-TENG which can directly generate DC energy without using the rectifier bridge by harvesting energy from unhealthy electrostatic breakdown has great potential as a lightweight, flexible, wearable, and comfortable energy-harvesting device in the future.

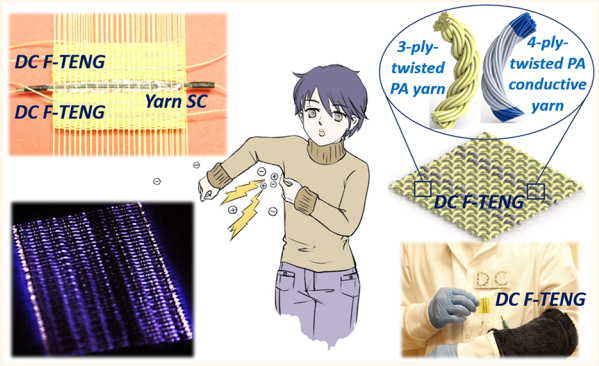

KEYWORDS: *direct current, fabric, triboelectric nanogenerator, energy harvesting, yarn supercapacitors*

The development and application of intelligent devices or wearable electronic products will continue to grow rapidly now and for the next decades.[1−5] Those devices focusing on human daily life, such as medical diagnosis sensors,[6,7] human interaction interfaces,[8] and human motion detection equipment,[9,10] are more functional and indispensable, which indicates that more energy is needed to ensure a person's normal life. Power transmitted from power plants to units is just part of the power needed for this world, so we have to rely on energy harvesting from the environment.[11] As the most common dispersed energy, human motion energy is the best choice for wearable electronics. Compared with other energy resources (coal and oil) and energy transfer mode (high voltage transmission for thousands of kilometers), human motion energy is sustainable, convenient, and efficient. Therefore, how to harvest biomotion energy becomes very important.

Triboelectric nanogenerators (TENGs) based on the coupling of electron transfer and electrostatic induction effects have attracted increasing attention and have developed rapidly in recent years.[12−14] Combined with textiles, TENGs have been used as various self-powered sensors, such as human-interactive and sensing devices,[15−18] pressure sensors[19,20] and acceleration sensors,[21] and almost all kinds of biomechanical energy-harvesting devices, such as walking, running, pulling, and bending.[22−27] However, most textile TENGs for energy harvest have to use stiff, uncomfortable, and unfriendly rectifier bridges to transfer alternating current (AC) to direct current (DC) to power electronic products. No matter how tiny the rectifier bridge is, it is a cold and power-wasting electronic component. Moreover, it is basically impossible for the existing textile technology to produce smart clothing with rectifier

Received: January 6, 2020
Accepted: March 17, 2020
Published: March 17, 2020

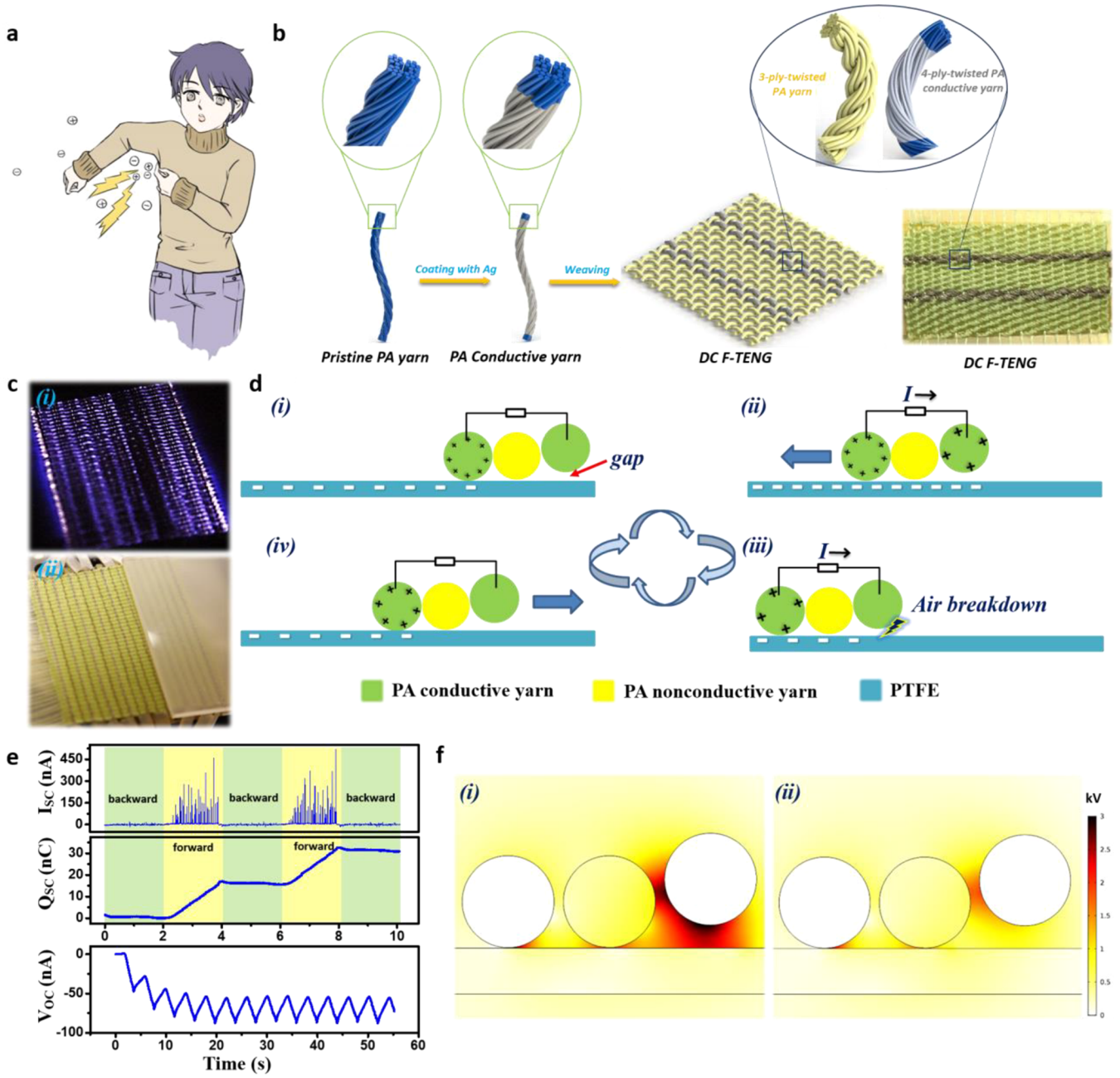

Figure 1. Schematic illustration, fabrication process, and working mechanism of the DC F-TENG. (a) Phenomenon of electrostatic breakdown of clothes in our daily life. (b) Fabrication process and schematic illustration of the DC F-TENG. (c) Photographs of the air break between the DC F-TENG and the polytetrafluoroethylene film during contact-sliding motion. (d) Schematic diagrams of the working principles of the DC F-TENG. (e) Representative electrical output performances of DC F-TENG, including short-circuit current, I_{SC}, short-circuit charge transfer, Q_{SC}, and open-circuit voltage, V_{OC}. (f) Simulated electric field distribution before and after electrostatic breakdown of the DC F-TENG.

bridges on a large scale and efficiently. At the same time, due to the high specific resistance of textile materials, how to improve antistatic performance is a traditional and hot research topic.[28−33] Based on some previous research about DC TENGs,[34−36] a DC fabric TENG (DC F-TENG) is developed.

Here, a DC F-TENG with the most common plain structure was designed to harvest biomotion energy by tactfully taking advantage of the harmful and annoying electrostatic breakdown phenomenon of clothes. The warp yarns of DC F-TENG are polyamide (PA, nylon-66) nonconductive yarn, and the weft yarns are composed of two kinds of yarns, PA nonconductive yarns and PA conductive yarns, which are separated as two electrodes (electrostatic breakdown yarns and frictional yarns). The influence of fabric structure parameters (16 different fabrics) on the output performance was systematically investigated by experimental testing and theoretical analysis. This kind of DC F-TENG can provide high DC output performances. A small DC F-TENG (1.5 cm × 3.5 cm) can easily light up 416 serially connected light-emitting diodes (LEDs). The V_{OC} (open-circuit voltage), I_{SC} (short-circuit current), and Q_{SC} (short-circuit charge transfer) of a bigger DC F-TENG (6.8 cm × 7 cm) can achieve about

https://dx.doi.org/10.1021/acsnano.0c00138
ACS Nano XXXX, XXX, XXX−XXX

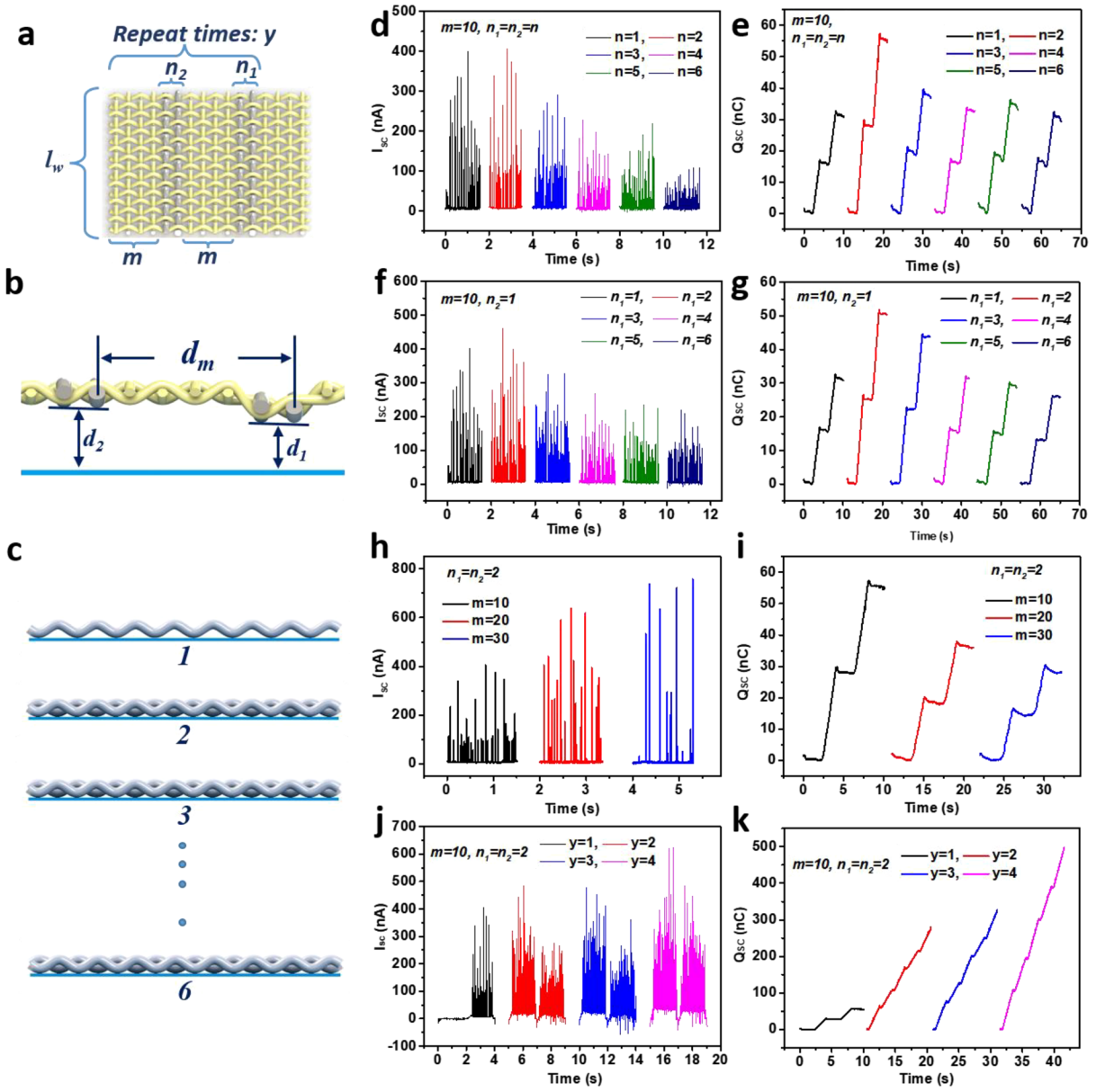

Figure 2. Influence of fabric structure parameters on the output performance of DC F-TENG. (a) Fabric structure parameters which can influence the output performances of DC F-TENG. (b) Direct physical factors which can influence the output performance of DC F-TENG. (c) Variation of contact area between PA conductive yarns and PTFE film with the increase of number (n_1) of the frictional yarns from 1 to 6. (d,e) Electrical output performances: (d) I_{SC} and (e) Q_{SC} with the increase of number (n) of electrostatic breakdown yarns and the frictional yarns from 1 to 6. (f,g) Electrical output performances: (f) I_{SC} and (g) Q_{SC} with the increase of number (n_1) of frictional yarns from 1 to 6. (h,i) Electrical output performances: (h) I_{SC} and (i) Q_{SC} with the increase of number (m) of PA nonconductive yarns from 10 to 30. (j,k) Electrical output performances: (j) I_{SC} and (k) Q_{SC} with the increase of repeat times (y) from 1 to 4.

4500 V, 40 μA, and 4.47 μC per motion cycle, respectively. Moreover, a solid-state yarn supercapacitor (SC) was fabricated by carbon fiber and poly(3,4-ethylenedioxythiophene):poly(styrenesulfonate) (PEDOT:PSS). Then the soft yarn SCs and PA yarns are woven as fabric SC. By directly connecting the fabric SC, as a whole wearable energy-harvesting and storage fabric, the DC F-TENG can continually provide DC energy to power a calculator or a hygrothermograph.

RESULTS AND DISCUSSION

Electrostatic breakdown, or air breakdown phenomenon, is a very common phenomenon when we rub clothes, such as wool-based fabrics, especially in very dry weather, as shown in Figure 1a. In most case, this is a negative effect. Because it is very hard to harvest the energy from electrostatic breakdown on garments, most researchers focus on how to eliminate this effect through complex chemical treatment on the surface of yarns and fabrics. Fortunately, based on the mechanism of electron transfer, the invention of TENGs shows the possibility to solve this problem. Some works have made progress in how to collect energy from electrostatic breakdown.

As shown in Figure 1b, a DC F-TENG is interwoven by warp yarns and weft yarns as a common plain structure. A three-ply twisted nonconductive PA yarn is chosen as the warp yarn because the PA yarn is a very widely used insulating textile material in the world and has high production and excellent

https://dx.doi.org/10.1021/acsnano.0c00138
ACS Nano XXXX, XXX, XXX−XXX

performance, such as high breaking strength and high abrasive resistance. The weft yarns are composed of two kinds of yarns, PA nonconductive yarns and PA conductive yarns, which are separated as two electrodes (electrostatic breakdown yarns and frictional yarns). The PA nonconductive yarn is used to separate the electrostatic breakdown yarns from the frictional yarns. A four-ply twisted PA yarn coated with Ag is used as the conductive yarn because of its perfect conductivity (0.5 Ω cm^{-1}). The diameters of PA conductive yarn and PA nonconductive yarn are 0.52 and 0.40 mm, as shown in Figure S1 (Supporting Information). The area density of the DC F-TENG is about 326 g/m^2, which is a lightweight normal fabric. By moving forward and backward on the surface of polytetrafluoroethylene (PTFE) film and connecting two electrodes, we can harvest DC energy continuously. The test method is demonstrated in detail in Figure S2 (Supporting Information). When we turn over the DC F-TENG and PTFE film (attached to the acrylic substrate), we can observe the phenomenon of air breakdown and point discharge by moving the acrylic substrate forward and backward. The existence of this phenomenon is confirmed by taking a photo with 30 s exposure in a dark room, as shown in Figure 1c-*i*. As a contrast, the original photograph with no air breakdown is present in Figure 1c-*ii*.

The special structure endows the DC F-TENG great properties for generating direct current by contacting and sliding with other things, such as a PTFE film and a commonly used fabric. The working mechanism of DC F-TENG based on air breakdown is illustrated in Figure 1d. For better understanding, we chose one woven unit (including one electrostatic breakdown electrode and one frictional electrode) to analyze the working mechanism.

Under the contact-sliding motion mode, at stage *i* of Figure 1d, the DC F-TENG slides from left to right and stops at the end of the right. The surface of the frictional electrode and PTFE film is charged with the same amount of opposite charges. The PTFE film is proven to be negatively charged because of its ability to attract more electrons than Ag. At stage *ii* in Figure 1d, when the DC F-TENG is moving from right to left under an external force, positive charges will slowly flow from the frictional electrode to the electrostatic breakdown electrode. So there will be a small DC of about 7.5 nA, as shown in Figure S3 (Supporting Information). The electric potential difference between the electrostatic breakdown of the electrode and PTFE film will increase during this contact-sliding motion. At stage *iii* in Figure 1d, once the electric potential difference exceeds the breakdown voltage (according to Paschen's law[37]), the air will begin conducting. A discharge between the PTFE film and the electrostatic breakdown electrode occurs due to the electrical breakdown of air. The electrons will flow from the PTFE film to the electrostatic breakdown electrode, and charge neutralization occurs. At this time, there will be a big electric potential difference between two electrodes, and the electric potential of the frictional electrode is higher than that of the electrostatic breakdown electrode. Then there will be a short (*e.g.*, about 0.005 s) and big current (*e.g.*, about 360 nA) flowing from the frictional electrode to electrostatic breakdown electrode, as shown in Figure S4a,b (Supporting Information). At the same time, there is a small voltage drop (*e.g.*, about 1.6 V), as shown in Figure S4c,d (Supporting Information). If the DC F-TENG continues to move toward the left, it will produce continuous direct current pulse outputs. At stage *iv* in Figure 1d, as long as the fabric reaches the far left side of the PTFE film and moves from left to right, the air breakdown will not happen anymore due to no electrons on the surface of the PTFE film directly below the electrostatic breakdown electrode. Then there are no positive charge transfers from the frictional electrode to the electrostatic breakdown electrode. As a result, if the DC F-TENG moves as cycles (*i*−*ii*−*iii*−*iv*), the electrons will always transfer from the frictional electrode to PTFE film, then to the electrostatic breakdown electrode, and then back to frictional electrode in turn. The representative electrical output performances of the DC F-TENG, including short-circuit current, I_{SC}, short-circuit charge transfer, Q_{SC}, and open-circuit voltage, V_{OC}, are demonstrated in Figure 1e. To obtain a more quantitative understanding, we establish a theoretical model of the DC F-TENG to observe the electric potential distribution of PTFE film and fabric before (Figure 1f-*i*) and after (Figure 1f-*ii*) air breakdown by a simple finite element simulation using COMSOL Multiphasic software. A detailed illustration of the charge distribution procedure can be found in Figure S5 (Supporting Information).

In Figure 2, in order to optimize the electrical output performances of the DC F-TENG, we systematically investigated the influence of fabric structure parameters, unit repeat times (y) and weft yarns' number (electrostatic breakdown yarn, n_1, the frictional yarn, n_2, and PA nonconducting yarn, m). For the accuracy of the test, all of these fabrics with different parameters have the same woven structure (plain woven fabric) and the same contact-sliding materials (PTFE film). The electrical output performances are measured using a linear motor to provide periodic contact-sliding movements.

In Figure 2d,e and Figure S6a (Supporting Information), six types of DC F-TENGs with one unit (y = 1, including one electrostatic breakdown electrode and one frictional electrode) are designed and tested to investigate the effect of row number of the yarns on the electrical output performance of DC F-TENGs, with n ($n_1 = n_2 = n$) increasing from 1 to 6. The row number of the PA nonconducting yarn remains unchanged (m = 10). That is, we fabricate six types of DC F-TENGs with two electrodes, with the area increasing at the same time and other structure parameters being unchanged. From Figure 2d,e, when n = 1 and n = 2, the I_{SC} is almost the same, and the Q_{SC} of DC F-TENG (n = 2) is almost twice as big as the Q_{SC} of DC F-TENG (n = 1). With the increase of n from 2 to 6, the I_{SC} and Q_{SC} both decrease. The results are consistent with the theoretical derivation in Supporting Information, Notes S1 and S2 (1). Therefore, the DC F-TENG (n_1 = 2, n_2 = 1, m = 10) has the highest output performances in these six fabrics.

In Figure S6b (Supporting Information), six types of DC F-TENGs with one unit (y = 1) are designed and tested to investigate the effect of row number of the frictional yarns on the electrical output performance of DC F-TENGs, with n_1 increasing from 1 to 6, m = 10, and n_2 = 1. That is, we fabricate six DC F-TENGs with only the frictional electrode area increasing and other structure parameters remaining unchanged. As shown in Figure 2f,g, when n_1 = 2, the I_{SC} and Q_{SC} is the biggest. With the increase of n_1 from 2 to 6, the I_{SC} and Q_{SC} both decrease. The results are consistent with the theoretical derivation in Supporting Information, Note S2 (2). Hence, the DC F-TENG (n_1 = 2, n_2 = 2, m = 10) has the highest output performances in these six fabrics.

In Figure S8a−c (Supporting Information), three types of DC F-TENGs with one unit (y = 1) are designed and tested to

https://dx.doi.org/10.1021/acsnano.0c00138
ACS Nano XXXX, XXX, XXX−XXX

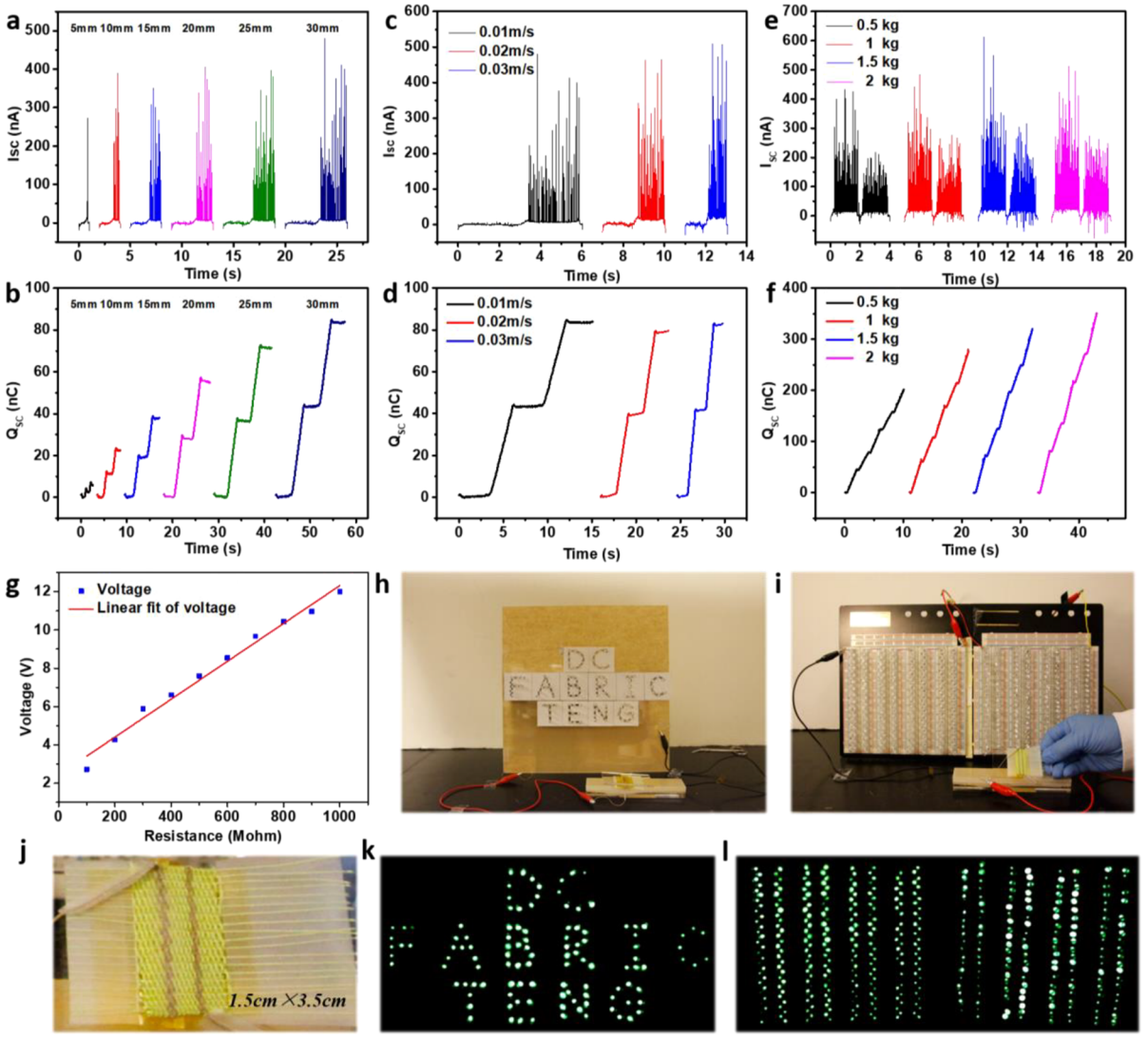

Figure 3. Influence of test conditions on the output performance and demonstrations of the ability to harvest energy from a DC F-TENG. (a,b) Electrical output performances: (a) I_{SC} and (b) Q_{SC} with the increase of different sliding distance from 5 to 30 mm. (c,d) Electrical output performances: (c) I_{SC} and (d) Q_{SC} with the increase of sliding speed from 0.01 to 0.03 m s^{-1}. (e,f) Electrical output performances: (e) I_{SC} and (f) Q_{SC} with the increase of weight from 1 to 4 kg. (g) Output voltage curve at different high resistance. (h) Photographs of words "DC FABRIC TENG" LEDs and DC energy-harvesting device. (i) Photographs of 416 LEDs and DC energy-harvesting device. (j) Enlarged photograph of the small DC F-TENG used to harvest energy in (h,i). (k) Demonstration of lighting up 115 LEDs marked as letters "DC FABRIC TENG". (l) Demonstration of lighting up 416 LEDs.

investigate the effect of the row number (m = 10,20 and 30) of the PA nonconductive yarns on the electrical output performance of DC F-TENGs. That is, we fabricate three DC F-TENGs with only the distance (d_m, Figure 2b) between two electrodes increasing and other structure parameters remaining unchanged ($n_1 = n_2 = 2$). As shown in Figure 2h,i, with the increase of m from 10 to 30, the I_{SC} increases from 400 to 760 nA, and the Q_{SC} decreases from 57 to 30 nC. The results of I_{SC} is consistent with the theoretical derivation in the Supporting Information Note S2 (3). According to Supporting Information Note S2 (3), the Q_{SC} should be the same, whereas, in fact, the charges will diffuse into air from the PTFE film. So the longer the time the charges stay on the surface, the more charges that escape into the air. That is the reason that the Q_{SC} decreases with increasing m. Therefore, we can conclude that when we only change d_m, the output I_{SC} will increase with increasing d_m, and Q_{SC} will decrease with increasing d_m.

In Figure S8a,d–f (Supporting Information), four types of DC F-TENGs with different units (y = 1, 2, 3, 4) are designed and tested to investigate the effect of the fabric woven units on the electrical output performances of DC F-TENGs. Other structure parameters are the same ($n_1 = n_2 = 2$, m = 10). As shown in Figure 2j,k, compared with the result of DC F-TENG with only one unit (y = 1), the I_{SC} and Q_{SC} change a lot. When the units are larger than one (y > 1), the DC F-TENG has direct current regardless of the moving direction (moving forward and backward), as well as the Q_{SC}. That is because some frictional electrodes have electrostatic breakdown electrodes on both sides. When the DC F-TENG moves forward and backward, air breakdown phenomenon will happen for same mechanism, as shown in Figure 1d. Based on the trend of the output in Figure 2j,k, we can conclude that the I_{SC} and Q_{SC} will increase with the unit increasing.

All of the test conditions for the measurement to investigate the influence of fabric structure parameters on the electric

https://dx.doi.org/10.1021/acsnano.0c00138
ACS Nano XXXX, XXX, XXX−XXX

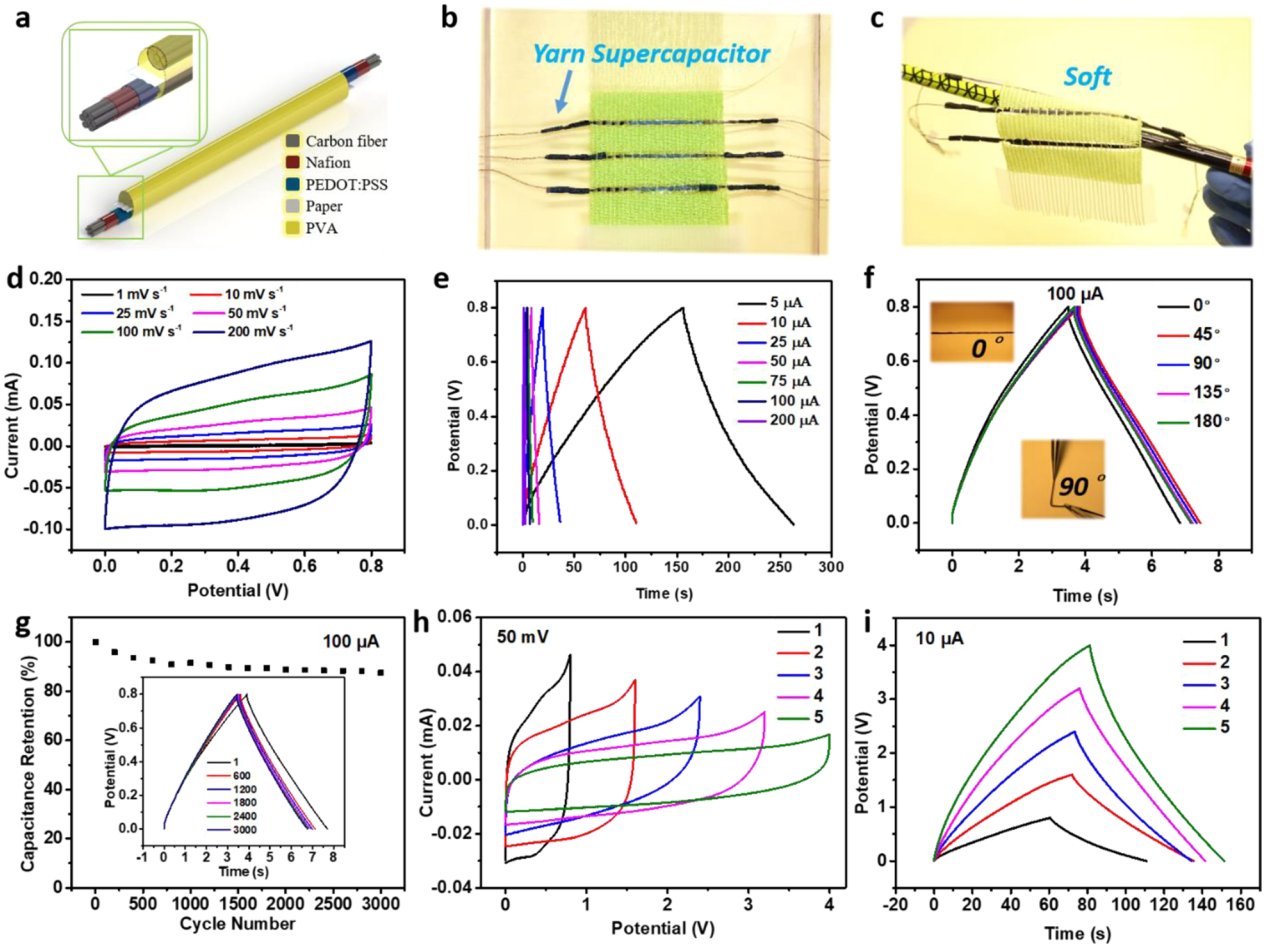

Figure 4. Schematic illustration and electrochemical characterization of the yarn SC. (a) Schematic illustration of the yarn SC and the detailed structure. (b) Photograph of the fabric SC woven by the PA yarn and the yarn SC. (c) Photograph of the fabric SC hanging on a pencil. (d) CV curves of the yarn SC under various scanning rates (1−200 mV s^{-1}). (e) GCD curves of the yarn SC at different current loadings (5−200 μA). (f) GCD curves of the yarn SC at different bending degrees (0−180°). (g) Long-term stability of the yarn SC for 3000 charging/discharging cycles. (h) CV curves of the yarn SC in series connection (1−5 SCs). (i) GCD curves of the yarn SC in series connection (1−5 SCs).

output performance are the same. That is, the weight on every frictional electrode is 1 kg; the moving velocity is 0.01 m s^{-1}, and the moving distance is 20 mm. All corresponding voltage curves of the test in Figure 2 are shown in Figures S9−S12 (Supporting Information).

In order to better understand the working mechanism of the DC F-TENG and to obtain higher output, we change the moving distance, velocity, and weight to investigate the influence of test conditions. Some DC F-TENGs are taken as the testing samples in Figure 3. The structure parameters of the DC F-TENG tested in Figure 3a−d,g are $n_1 = n_2 = 2$, $m = 10$, and $y = 1$. The structure parameters of the DC F-TENG tested in Figure 3e,f are $n_1 = n_2 = 2$, $m = 10$, and $y = 2$. As shown in Figure 3a,b, where moving velocity is 0.01 m s^{-1} and weight is 1 kg, the I_{SC} almost remains at the same value (about 0.4 μA) and the Q_{SC} will increase linearly with the moving distance increasing from 5 to 30 mm. As presented in Figure 3c,d, where the moving distance is 30 mm and weight is 1 kg, I_{SC} and Q_{SC} remain unchanged. It is clear that different moving velocity will not affect the electrical output performances of the DC F-TENG too much for every motion cycle. As demonstrated in Figure 3e,f, where the moving distance is 30 mm and moving velocity is 0.01 m s^{-1}, the I_{SC} increases slightly and the Q_{SC} increases linearly with the weight increasing from 0.5 to 2 kg on every frictional electrode. In a word, when the structure parameters of the DC F-TENG are not changed, the I_{SC} will increase only when the weight increases. The Q_{SC} will be improved when the moving distance and weight increase. All corresponding voltage curves of the test in Figure 3a−f are shown in Figures S13−S15 (Supporting Information). As shown in Figure 3g, the voltage drops on the resistance nearly increases with the load linearly when the load resistance increases from 100 to 1000 MΩ. The good linearity exhibits a stable DC output with this kind of TENG at a high load resistance. In order to prove the output current is DC and to demonstrate the ability of this DC F-TENG as a power source, some movies are provided with this paper. As shown in Figure 3h and Movie S1, when we slide the small DC F-TENG (Figure 3j, enlarged view of the DC F-TENG in Figure 3i) with PTFE film, "DC FABRIC TENG" (115 LEDs) can be sufficiently lighted up. However, no light emission can be observed when the two electrodes are connected to the device with reversed polarity, which directly proves that the output is DC. When we connect the small DC F-TENG with 416 LEDs on two breadboards (Figure 3i), these LEDs can be easily

https://dx.doi.org/10.1021/acsnano.0c00138
ACS Nano XXXX, XXX, XXX−XXX

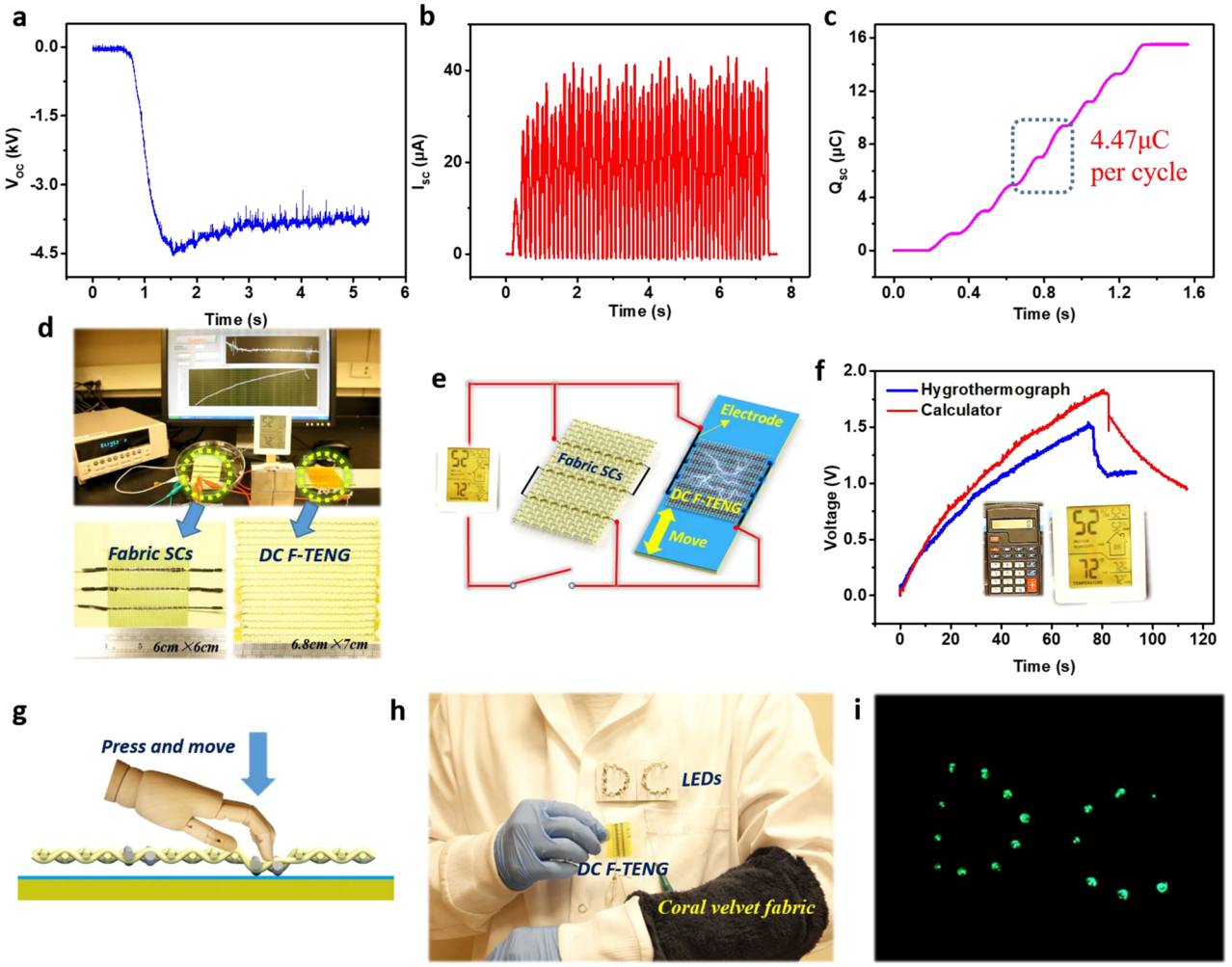

Figure 5. Applications and electrical output performances of the DC F-TENG. (a–c) High electrical output performance: (a) I_{SC}, (b) V_{OC}, and (c) Q_{SC} of the DC F-TENG (6.8 cm × 7 cm). (d) Demonstration of charging the fabric SC (6 cm × 6 cm) by DC F-TENG (6.8 cm × 7 cm) to power a hygrothermograph. (e) Circuit diagram of the self-charging textile integrated by the DC F-TENG and fabric SCs. (f) Charging curves of fabric SCs (three in series) by DC F-TENG. The inset pictures are a calculator (left) and a hygrothermograph (right) powered by the fabric SC. (g) Schematic illustration of driving the DC F-TENG by hand. (h,i) Photograph demonstration that LEDs marked with letters "DC" can be lighted up by sliding the DC F-TENG with a coral velvet fabric on the wrist.

lighted up, which indicates the high output performances of the DC F-TENG (Figure 3l and Movie S2).

Yarn and fabric SC were fabricated to store energy for the DC F-TENG. Figure 4a shows the schematic illustration of the yarn SC. The yarn SC consists of two parallel bunches of carbon fibers (Figure S16a, Supporting Information) coated with Nafion and PEDOT:PSS and solid-state H_3PO_4/poly-(vinyl alcohol) (PVA) gel as the electrolyte (Figure S16b, Supporting Information). The detailed fabrication processes can be found in the Methods section. This flexible yarn SC can be easily woven as a fabric SC (Figure 4b and Figure S16c, Supporting Information) or fabricated with the DC F-TENG as a whole self-charging power system Figure S16d, Supporting Information). Figure 4c presents the good flexibility and perfect softness of the fabric SC. To confirm the capacitive storage performance of the yarn SC, the electrochemical capacitance properties of this yarn SC are measured by cyclic voltammetry (CV), galvanostatic charging/discharging (GCD), and electrochemical impedance spectroscopy (EIS) techniques without a reference electrode. In Figure 4d, the rectangle-like CV curves of the yarn SC under various scanning rates (1–200 mV/s) have two peaks when potential is 0 and 0.8 V, which indicates faradaic pseudocapacitance characteristic of this yarn SC. The large slightly gradient plateau of the CV curves shows a good capacitive behavior. The GCD curves of the yarn SC at different current loadings (5–200 μA) are shown in Figure 4e. All of the curves are nearly symmetrical triangle-shaped, and the small IR voltage drop (ohm drop, 23 mV for 5 μA) shows high electrical conductivity of the electrodes. The mechanical and electrochemical stability are important for wearable products. As shown in Figure 4f, the GCD property is measured under different bending angles (0, 45, 90, 135, and 180°). Almost no obvious change is observed in the charge–discharge curves at a current loading 100 μA, indicating the great flexibility of the yarn SC. Figure 4g shows that the great durability that the capacitance retention is 87.5% after 3000 charging/discharging cycles at a current loading of 100 μA. According to the CV curves with different highest voltages (0.8, 1.0, 1.2, 1.4, 1.6 V), the highest working voltage should be set as 0.8 V (Figure S17a, Supporting Information) for the good performance of the CV curve at 0.8 V. By being woven in a plain woven fabric, the mechanical stability will be improved for the very stable plain structure of woven fabric. Therefore, the yarn SC and the fabric SC can maintain their

https://dx.doi.org/10.1021/acsnano.0c00138
ACS Nano XXXX, XXX, XXX–XXX

good mechanical and electrochemical performances in our daily life. The Nyquist plot of the Faber SC is tested by EIS from 0.01 Hz to 10 kHz, as presented in Figure S17d (Supporting Information). There is no obvious semicircle at high frequencies, indicating that there is a good electrical contact between the carbon fibers and H_3PO_4/PVA.

In addition, in order to satisfy different rated voltage and power requirements for different electronic devices, some yarn SCs are connected in series for higher voltage supply and parallel for higher power supply. With the way we wove the yarn SCs with free electrodes (Figure 4b), we can change the connection method (in series or parallel) to power different electronic products. The CV and GCD curves of the yarn SCs connected in series with different numbers (1 to 5) are displayed in Figure 4h,i, respectively. The good electrochemical behavior of yarn SCs connected in series demonstrates that these yarn SCs provide higher voltage and work well by increasing the number of them. On the other hand, these yarn SCs can offer larger capacitance by connecting in parallel, as shown in Figure S17b,c (Supporting Information). The Nyquist plots of the Faber SC connected in series and parallel are shown in Figure S17e,f (Supporting Information). In one word, free combination and excellent stability give these yarn SCs a wide range of applications.

A DC F-TENG ($n_1 = n_2 = 2$, $m = 10$, $y = 8$) with large size (6.8 cm × 7 cm) was woven, as shown in Figure S18a (Supporting Information) and Figure 5d (lower right corner). The V_{OC}, I_{SC}, and Q_{SC} of this large DC F-TENG (6.8 cm × 7 cm) can easily achieve about 4500 V, 40 μA, and 4.47 μC per motion cycle, respectively, as shown in Figure 5a−c. Combined with the fabric SC (3 yarn SCs in series), the energy harvested from human motion by the DC F-TENG can be directly stored in the fabric SC without a rectifier bridge or diodes, which can make it possible to drive wearable electronics. As presented in Figure 5d and Movie S3, through sliding the DC F-TENG on the surface of the PTFE film in a short time about of 1 min and 10 s, a hygrothermograph can work in about 10 s. In Figure S18b and Movie S4 (Supporting Information), through sliding the DC F-TENG on the surface of PTFE film in about 1 min and 20 s, a calculator can be turned on with a "beep" sound. After we turn off the voice switch, the calculator can give a right answer "16" when we input "8" plus "8". The circuit design of the self-charge power system is very simple and efficient, as shown in Figure 5e. This simple circuit can transfer human motion energy into electric energy efficiently without losing energy in other electronic components. The real time voltage curves of fabric SC are shown in Figure 5f when we use the self-charge power system to power the hygrothermograph and calculator. The insets in Figure 5f are the operating state of the hygrothermograph and the calculator. In our daily life use, we can also drive the DC F-TENG by our hand without using any press plate, as shown in Figure S2c (Supporting Information). As shown in Figure 5g, we can press and move the DC F-TENG by our hand on the surface of a film or fabric. In Figure 5h,i and Movie S5 (Supporting Information), the LEDs marked with the letters "DC" can be lighted up by sliding the DC F-TENG on a coral velvet fabric (PET fabric). All of the demonstrations and data indicate that this self-charge power system consisting of a DC F-TENG and fabric SCs has wonderful potential applications as a sustainable and eco-friendly power source for wearable devices.

CONCLUSION

In summary, a direct current fabric triboelectric nanogenerator (DC F-TENG) with the most common plain structure is designed to harvest biomotion energy by tactfully taking advantage of the harmful and annoying electrostatic breakdown phenomenon of clothes. This kind of DC F-TENG consists of common PA yarns as warp and weft yarns and PA conductive yarns as weft yarns. Sixteen fabrics are woven to systematically investigate the influence of structure parameters and test conditions on the output performances of the DC fabric-based TENG by experimental testing and theoretical analysis. A small size (1.5 cm × 3.5 cm) DC F-TENG can easily light up 416 LEDs, and the V_{OC}, I_{SC}, and Q_{SC} of a larger DC F-TENG (6.8 cm × 7 cm) can achieve about 4500 V, 40 μA, and 4.47 μC per motion cycle, respectively. Moreover, due to the special working mechanism, the DC F-TENG shows an efficient energy conversion by harvesting human motion energy and directly storing it in fabric SCs without any rectifier bridge or diode. In this self-charge power system, a hygrothermograph or a calculator can work well only after less than 1.5 min of human motion energy harvesting. With the consideration of this excellent performance, the low cost and high efficiency of the DC F-TENG has great potential as a lightweight, flexible, wearable, and comfortable energy-harvesting device in the future. Furthermore, this work provides a significative direction for textile-based TENG in harvesting direct current energy by making use of the air breakdown phenomenon and enabling its promising use in power supplies.

METHODS

Fabrication of the DC F-TENG. This DC F-TENG is easily fabricated by using a self-designed mold. It imitates the mature manufacturing technique which has already existed in the textile field for a long time and was suitable for large-area industrial production. It is woven by weft yarns and warp yarns. The warp yarn (PA yarn) is wound around the self-designed mode with 20 rows. The weft yarn (PA yarn, PA yarn coated with Ag) is interwoven with the warp yarn every other yarn.

Fabrication of the Yarn SC. The carbon fiber bundles were first ultrasonically cleaned in acetone, ethanol, and deionized water for 10 min. After the carbon fiber bundles were dried in an 80 °C oven for 30 min, the carbon fiber bundles were homogeneously coated with Nafion alcohol solution and dried again in the oven. PEDOT:PSS was mixed with ethylene glycol and Triton X-100 under sonication for 5 min. Then, PEDOT:PSS was drop-coated on the carbon fibers, followed by annealing at 100 °C for 20 min. The procedures were repeated twice to increase the loading of PEDOT:PSS. Two as-prepared carbon-fiber-based electrodes were coated with PVA/H_3PO_4 (1 g of PVA and 1 g of H_3PO_4 in 10 mL of deionized water) gel electrolyte and assembled with a cellulose separator. After the PVA/H_3PO_4 gel solidified at room temperature, the flexible yarn SC was obtained.

Device Characterizations. The surface morphology of the silver-coated PA yarn, as well as PA nonconductive yarn, was characterized with a field emission scanning electron microscope (SU-8010, Hitachi). The electrical output (V_{OC}, I_{SC}, and Q_{SC}) of the fabric-based TENG during sliding was implemented by a linear motor and an electrometer (Keithley 6514 system).

ASSOCIATED CONTENT

Supporting Information

The Supporting Information is available free of charge at https://pubs.acs.org/doi/10.1021/acsnano.0c00138.

Figures S1−S18 and Notes S1 and S2; SEM images, test method, representative electrical output of DC, detailed

https://dx.doi.org/10.1021/acsnano.0c00138
ACS Nano XXXX, XXX, XXX−XXX

working principles, photographs of all DC F-TENG, electrical output performance of V_{OC}, electrochemical characterization of the fiber SC; theoretical derivation of electrical output of DC F-TENG with different parameters (PDF)

Movie S1: Demonstration of lighting LED letters by DC F-TENG (AVI)

Movie S2: Demonstration of lighting 416 LEDs by DC F-TENG (AVI)

Movie S3: Demonstration of lighting a hygrothermograph by DC F-TENG (AVI)

Movie S4: Demonstration of lighting a calculator by DC F-TENG (AVI)

Movie S5: Demonstration of lighting "DC" LEDs by DC F-TENG sliding on a coral velvet fabric (AVI)

AUTHOR INFORMATION

Corresponding Authors

Zhaoqun Du − *Key Laboratory of Textile Science & Technology, Ministry of Education, College of Textiles, Donghua University, Shanghai 201620, P.R. China;* orcid.org/0000-0003-1878-642X; Email: duzq@dhu.edu.cn

Zhong Lin Wang − *School of Material Science and Engineering, Georgia Institute of Technology, Atlanta, Georgia 30332, United States; Beijing Institute of Nanoenergy and Nanosystems, Chinese Academy of Sciences, Beijing 100083, P.R. China;* orcid.org/0000-0002-5530-0380; Email: zhong.wang@mse.gatech.edu

Authors

Chaoyu Chen − *School of Material Science and Engineering, Georgia Institute of Technology, Atlanta, Georgia 30332, United States; Key Laboratory of Textile Science & Technology, Ministry of Education, College of Textiles, Donghua University, Shanghai 201620, P.R. China*

Hengyu Guo − *School of Material Science and Engineering, Georgia Institute of Technology, Atlanta, Georgia 30332, United States*

Lijun Chen − *School of Material Science and Engineering, Georgia Institute of Technology, Atlanta, Georgia 30332, United States; Key Laboratory of Textile Science & Technology, Ministry of Education, College of Textiles, Donghua University, Shanghai 201620, P.R. China*

Yi-Cheng Wang − *Department of Food Science and Human Nutrition, University of Illinois at Urbana—Champaign, Urbana, Illinois 61801, United States*

Xianjie Pu − *Department of Applied Physics, State Key Laboratory of Power Transmission Equipment & System Security and New Technology, Chongqing University, Chongqing 400044, P.R. China*

Weidong Yu − *Key Laboratory of Textile Science & Technology, Ministry of Education, College of Textiles, Donghua University, Shanghai 201620, P.R. China*

Fumei Wang − *Key Laboratory of Textile Science & Technology, Ministry of Education, College of Textiles, Donghua University, Shanghai 201620, P.R. China*

Complete contact information is available at: https://pubs.acs.org/10.1021/acsnano.0c00138

Author Contributions

[#]C.C., H.G., and L.C. contributed equally to this work.

Notes

The authors declare no competing financial interest.

ACKNOWLEDGMENTS

The authors are grateful for the support received by the Fundamental Research Funds for the Central Universities (2232018G-01) and by Graduate Student Innovation Fund of Donghua University (CUSF-DH-D-2019031). This work is also supported by the Hightower Chair Foundation of Georgia Institute of Technology of USA. C.C. and L.C. acknowledge the China Scholarship Council for supporting research at Georgia Institute of Technology.

REFERENCES

(1) Fan, F.-R.; Tian, Z.-Q.; Wang, Z. L. Flexible Triboelectric Generator! *Nano Energy* **2012**, *1*, 328−334.

(2) Stoppa, M.; Chiolerio, A. Wearable Electronics and Smart Textiles: A Critical Review. *Sensors* **2014**, *14*, 11957−11992.

(3) Fan, F. R.; Tang, W.; Wang, Z. L. Flexible Nanogenerators for Energy Harvesting and Self-Powered Electronics. *Adv. Mater.* **2016**, *28*, 4283−4305.

(4) Zamarayeva, A. M.; Ostfeld, A. E.; Wang, M.; Duey, J. K.; Deckman, I.; Lechêne, B. P.; Davies, G.; Steingart, D. A.; Arias, A. C. Flexible and Stretchable Power Sources for Wearable Electronics. *Sci. Adv.* **2017**, *3*, No. e1602051.

(5) Zhong, J.; Zhang, Y.; Zhong, Q.; Hu, Q.; Hu, B.; Wang, Z. L.; Zhou, J. Fiber-Based Generator for Wearable Electronics and Mobile Medication. *ACS Nano* **2014**, *8*, 6273−6280.

(6) Liu, Z.; Ma, Y.; Ouyang, H.; Shi, B.; Li, N.; Jiang, D.; Xie, F.; Qu, D.; Zou, Y.; Huang, Y.; et al. Transcatheter Self-Powered Ultrasensitive Endocardial Pressure Sensor. *Adv. Funct. Mater.* **2019**, *29*, 1807560.

(7) Kim, J.; Campbell, A. S.; de Ávila, B. E.-F.; Wang, J. Wearable Biosensors for Healthcare Monitoring. *Nat. Biotechnol.* **2019**, *37*, 389−406.

(8) Jung, S.; Kim, J. H.; Kim, J.; Choi, S.; Lee, J.; Park, I.; Hyeon, T.; Kim, D. H. Reverse-Micelle-Induced Porous Pressure-Sensitive Rubber for Wearable Human−Machine Interfaces. *Adv. Mater.* **2014**, *26*, 4825−4830.

(9) Dong, K.; Wu, Z.; Deng, J.; Wang, A. C.; Zou, H.; Chen, C.; Hu, D.; Gu, B.; Sun, B.; Wang, Z. L. A Stretchable Yarn Embedded Triboelectric Nanogenerator as Electronic Skin for Biomechanical Energy Harvesting and Multifunctional Pressure Sensing. *Adv. Mater.* **2018**, *30*, 1804944.

(10) Yamada, T.; Hayamizu, Y.; Yamamoto, Y.; Yomogida, Y.; Izadi-Najafabadi, A.; Futaba, D. N.; Hata, K. A Stretchable Carbon Nanotube Strain Sensor for Human-Motion Detection. *Nat. Nanotechnol.* **2011**, *6*, 296.

(11) Wang, Z. L. Entropy Theory of Distributed Energy for Internet of Things. *Nano Energy* **2019**, *58*, 669−672.

(12) Wang, Z. L.; Wang, A. C. On the Origin of Contact-Electrification. *Mater. Today* **2019**, *30*, 34−51.

(13) Wang, Z. L. Triboelectric Nanogenerators as New Energy Technology and Self-Powered Sensors - Principles, Problems and Perspectives. *Faraday Discuss.* **2014**, *176*, 447−458.

(14) Liu, G.; Chen, J.; Tang, Q.; Feng, L.; Yang, H.; Li, J.; Xi, Y.; Wang, X.; Hu, C. Wireless Electric Energy Transmission through Various Isolated Solid Media Based on Triboelectric Nanogenerator. *Adv. Eng. Mater.* **2018**, *8*, 1703086.

(15) Dong, K.; Deng, J.; Ding, W.; Wang, A. C.; Wang, P.; Cheng, C.; Wang, Y. C.; Jin, L.; Gu, B.; Sun, B.; et al. Versatile Core−Sheath Yarn for Sustainable Biomechanical Energy Harvesting and Real-Time Human-Interactive Sensing. *Adv. Eng. Mater.* **2018**, *8*, 1801114.

(16) Lai, Y. C.; Deng, J.; Zhang, S. L.; Niu, S.; Guo, H.; Wang, Z. L. Single-Thread-Based Wearable and Highly Stretchable Triboelectric Nanogenerators and Their Applications in Cloth-Based Self-Powered

https://dx.doi.org/10.1021/acsnano.0c00138
ACS Nano XXXX, XXX, XXX−XXX

Human-Interactive and Biomedical Sensing. *Adv. Funct. Mater.* **2017**, *27*, 1604462.
(17) Xie, L.; Chen, X.; Wen, Z.; Yang, Y.; Shi, J.; Chen, C.; Peng, M.; Liu, Y.; Sun, X. Spiral Steel Wire Based Fiber-Shaped Stretchable and Tailorable Triboelectric Nanogenerator for Wearable Power Source and Active Gesture Sensor. *Nano-Micro Lett.* **2019**, *11*, 39.
(18) Yang, Y.; Sun, N.; Wen, Z.; Cheng, P.; Zheng, H.; Shao, H.; Xia, Y.; Chen, C.; Lan, H.; Xie, X.; et al. Liquid-Metal-Based Super-Stretchable and Structure-Designable Triboelectric Nanogenerator for Wearable Electronics. *ACS Nano* **2018**, *12*, 2027−2034.
(19) Liu, M.; Pu, X.; Jiang, C.; Liu, T.; Huang, X.; Chen, L.; Du, C.; Sun, J.; Hu, W.; Wang, Z. L. Large-Area All-Textile Pressure Sensors for Monitoring Human Motion and Physiological Signals. *Adv. Mater.* **2017**, *29*, 1703700.
(20) Li, X.; Lin, Z.-H.; Cheng, G.; Wen, X.; Liu, Y.; Niu, S.; Wang, Z. L. 3D Fiber-Based Hybrid Nanogenerator for Energy Harvesting and as a Self-Powered Pressure Sensor. *ACS Nano* **2014**, *8*, 10674−10681.
(21) He, X.; Zi, Y.; Guo, H.; Zheng, H.; Xi, Y.; Wu, C.; Wang, J.; Zhang, W.; Lu, C.; Wang, Z. L. A Highly Stretchable Fiber-Based Triboelectric Nanogenerator for Self-Powered Wearable Electronics. *Adv. Funct. Mater.* **2017**, *27*, 1604378.
(22) Chen, J.; Huang, Y.; Zhang, N.; Zou, H.; Liu, R.; Tao, C.; Fan, X.; Wang, Z. L. Micro-Cable Structured Textile for Simultaneously Harvesting Solar and Mechanical Energy. *Nat. Energy* **2016**, *1*, 16138.
(23) Dong, K.; Deng, J.; Zi, Y.; Wang, Y. C.; Xu, C.; Zou, H.; Ding, W.; Dai, Y.; Gu, B.; Sun, B.; et al. 3D Orthogonal Woven Triboelectric Nanogenerator for Effective Biomechanical Energy Harvesting and as Self-Powered Active Motion Sensors. *Adv. Mater.* **2017**, *29*, 1702648.
(24) Xiong, J.; Cui, P.; Chen, X.; Wang, J.; Parida, K.; Lin, M.-F.; Lee, P. S. Skin-Touch-Actuated Textile-Based Triboelectric Nanogenerator with Black Phosphorus for Durable Biomechanical Energy Harvesting. *Nat. Commun.* **2018**, *9*, 4280.
(25) Chen, C.; Chen, L.; Wu, Z.; Guo, H.; Yu, W.; Du, Z.; Wang, Z. L. 3D Double-Faced Interlock Fabric Triboelectric Nanogenerator for Bio-Motion Energy Harvesting and as Self-Powered Stretching and 3D Tactile Sensors. *Mater. Today* **2020**, *32*, 84−93.
(26) Zhou, T.; Zhang, C.; Han, C. B.; Fan, F. R.; Tang, W.; Wang, Z. L. Woven Structured Triboelectric Nanogenerator for Wearable Devices. *ACS Appl. Mater. Interfaces* **2014**, *6*, 14695−14701.
(27) Wen, Z.; Yeh, M.-H.; Guo, H.; Wang, J.; Zi, Y.; Xu, W.; Deng, J.; Zhu, L.; Wang, X.; Hu, C.; et al. Self-Powered Textile for Wearable Electronics by Hybridizing Fiber-Shaped Nanogenerators, Solar Cells, and Supercapacitors. *Sci. Adv.* **2016**, *2*, No. e1600097.
(28) Bai, G.; Liu, Y. Antistatic Property of Polyacrylonitrile Fiber by Plasma-Grafting Treatment. *Text. Res. J.* **2010**, *80*, 1658−1664.
(29) Zhang, C.; Zhong, L.; Wang, D.; Zhang, F.; Zhang, G. Anti-Ultraviolet and Anti-Static Modification of Polyethylene Terephthalate Fabrics with Graphene Nanoplatelets by a High-Temperature and High-Pressure Inlaying Method. *Text. Res. J.* **2019**, *89*, 1488−1499.
(30) Shyr, T.-W.; Lien, C.-H.; Lin, A.-J. Coexisting Antistatic and Water-Repellent Properties of Polyester Fabric. *Text. Res. J.* **2011**, *81*, 254−263.
(31) Holdstock, P. The Damaging Effects of Electrostatic Discharges from Textile Surfaces. *J. Electrost.* **1997**, *40*, 529−534.
(32) Hersh, S. P. The Electrostatic Characteristics of Textile Materials. *Polym.-Plast. Technol. Eng.* **1974**, *3*, 29−48.
(33) Li, C.; Liang, T.; Lu, W.; Tang, C.; Hu, X.; Cao, M.; Liang, J. Improving the Antistatic Ability of Polypropylene Fibers by Inner Antistatic Agent Filled with Carbon Nanotubes. *Compos. Sci. Technol.* **2004**, *64*, 2089−2096.
(34) Liu, D.; Yin, X.; Guo, H.; Zhou, L.; Li, X.; Zhang, C.; Wang, J.; Wang, Z. L. A Constant Current Triboelectric Nanogenerator Arising from Electrostatic Breakdown. *Sci. Adv.* **2019**, *5*, No. eaav6437.
(35) Yang, Y.; Zhang, H.; Wang, Z. L. Direct-Current Triboelectric Generator. *Adv. Funct. Mater.* **2014**, *24*, 3745−3750.
(36) Luo, J.; Xu, L.; Tang, W.; Jiang, T.; Fan, F. R.; Pang, Y.; Chen, L.; Zhang, Y.; Wang, Z. L. Direct-Current Triboelectric Nanogenerator Realized by Air Breakdown Induced Ionized Air Channel. *Adv. Eng. Mater.* **2018**, *8*, 1800889.
(37) Boyle, W.; Kisliuk, P. Departure from Paschen's Law of Breakdown in Gases. *Phys. Rev.* **1955**, *97*, 255.

https://dx.doi.org/10.1021/acsnano.0c00138
ACS Nano XXXX, XXX, XXX−XXX